Journal of Controlled Release 300 (2019) 13–21

Contents lists available at ScienceDirect

Journal of Controlled Release

journal homepage: www.elsevier.com/locate/jconrel

Reductively cleavable polymer-drug conjugates based on dendritic polyglycerol sulfate and monomethyl auristatin E as anticancer drugs

Nadine Rades[a,b], Katharina Achazi[a], Min Qiu[b], Chao Deng[b], Rainer Haag[a], Zhiyuan Zhong[b,*], Kai Licha[a,*]

[a] Institute for Chemistry and Biochemistry, Freie Universität Berlin, Takustr. 3, Berlin 14195, Germany
[b] Biomedical Polymers Laboratory, Jiangsu Key Laboratory of Advanced Functional Polymer Design and Application, College of Chemistry, Chemical Engineering and Materials Science, Soochow University, Suzhou 215123, China

ARTICLE INFO

Keywords:
Polymer drug conjugates
Dendritic polyglycerol
Monomethyl auristatin E
Stimuli-responsive
Anticancer

ABSTRACT

Stimuli-responsive polymer-drug conjugates (PDCs) provide promising approaches in anticancer treatment. Here, we report the synthesis and biological evaluation of PDCs made of the highly potent antimitotic agent monomethyl auristatin E conjugated to dendritic polyglycerol and dendritic polyglycerol sulfate via a reductively cleavable, self-immolative disulfide linker. Cell viability assays with the human cancer cell lines A549 (lung carcinoma) and HeLa (cervix carcinoma) revealed that the drug's cytotoxicity was reduced by conjugation to the polymers, with the sulfated conjugates being more effective than the non-sulfated ones. Kinetic studies using real-time cell analysis indicated a retarded drug release from the polymers, with a much later cytotoxic response after treatment with the non-sulfated conjugates due to less cellular uptake, as confirmed by flow cytometry and confocal laser scanning microscopy. In contrast, the non-cleavable dPGS-MMAE conjugate that was synthesized for comparison was not cytotoxic under the same conditions. Overall, reductively cleavable dPGS-SS-MMAE conjugates showed promising results in vitro and good tolerability in vivo. Further in vivo studies are planned.

1. Introduction

The development of selective and effective anticancer drugs based on synthetic design remains a challenge in medicinal chemistry. The majority of clinically applied, low molecular weight anticancer drugs are hydrophobic, thus not water-soluble, and suffer from a short half-life in the blood stream and a high clearance rate. Additionally, they rapidly diffuse not only into tumor but also into healthy tissue. Thus, relatively small amounts reach the target site, and side effects occur due to the lack of any inherent selectivity for the tumor cell. To overcome these limitations, today's small molecular weight drugs are made selective by conjugating them to antibodies, peptides, or polymers, or physically encapsulating them into polymeric micelles, liposomes, or polymersomes. Both passive and active targeting strategies are used to redirect anticancer drugs. Active targeting is achieved by receptor-specific antibodies, proteins, and peptides, whereas liposomes, micelles, and other nanoparticles accumulate in tumor tissue due to enhanced permeation and retention (EPR effect). Drug release often happens upon a certain trigger that is present in tumor cells but negligible in healthy cells such as a low pH value, high redox potential, or the presence of specific enzymes. The progress, challenges, and opportunities in the field of cancer nanomedicine were reviewed extensively by Wicki et al. in 2015 [1], and a more recent review was published in 2017 by Shi et al. [2]. The most successful nanomedicine therapeutics in clinical cancer care are antibody-drug conjugates (ADCs) and liposomal drugs. Polymer-drug conjugates (PDCs) with antitumor activity are not on the market so far, but several are in clinical trials. Most of them are HPMA- or PEG-drug conjugates [1]. Beside such linear polymers, dendritic polymers are of great interest within the research community, including poly(amido amine) (PAMAM) [3,4], poly(ethylene imine) (PEI) [5,6], and dendritic polyglycerol (dPG) [7,8].

dPG-based polymers are a class of fully synthetic, highly biocompatible, and water-soluble macromolecular compounds. To date, functionalized and post-modified dPG has been examined, for example, as coatings for biomedical devices or biosensors, as drug carriers, components in hydrogels, and as an alternative to natural macromolecules such as human serum albumin (HSA) or heparin [7]. Sulfated dPG, dendritic polyglycerol sulfate (dPGS), was originally investigated to mimic natural polysulfates such as heparin. dPGS can be easily obtained from dPG by a simple sulfation process. Due to the new

* Corresponding authors.
E-mail addresses: zyzhong@suda.edu.cn (Z. Zhong), kai.licha@fu-berlin.de (K. Licha).

https://doi.org/10.1016/j.jconrel.2019.01.035
Received 2 October 2018; Received in revised form 18 January 2019; Accepted 24 January 2019
Available online 19 February 2019
0168-3659/

properties implemented by sulfation, dPGS was further examined as anti-inflammatory agent. Moreover, dPGS was studied as a carrier for the anticancer drug paclitaxel that was covalently bound via acid labile functional groups [9,10].

In our approach, we used another tubulin inhibitor that is much more effective than paclitaxel, namely, monomethyl auristatin E (MMAE), and a reductively cleavable disulfide linkage. MMAE is known from the approved ADC brentuximab vedotin which is used to treat relapsed or refractory Hodgkin lymphoma and systemic anaplastic large cell lymphoma [11]. Here, MMAE is bound covalently to the anti-CD30 monoclonal antibody cAC10 via a maleimidocaproyl-valine-citrulline-*p*-aminobenzyloxycarbonyl linker (cAC10-Val-Cit-MMAE or cAC10-MC-Val-Cit-PABC-MMAE). The valine-citrulline linker can be cleaved off by proteases such as human cathepsin B, and the *p*-aminobenzyloxycarbonyl spacer is a self-immolative moiety. As a result, the parent drug MMAE is released after proteolytic cleavage and subsequent self-immolation [12]. In general, the high selectivity and specificity of an antibody leads to fewer side effects, but usually only few cancer types can be targeted with one ADC, always depending on the respective receptor status. A carrier-drug conjugate with a polymer as a carrier instead of an antibody should be applicable more generally against a variety of tumor types by passive targeting. Fig. 1 illustrates our approach, utilizing a well known reductively cleavable and self-immolative disulfide linker [13–15], to finally liberate the parent drug molecule without a portion of the linker.

2. Materials and methods

2.1. Materials

All chemicals were of analytical grade and used as received unless otherwise noted. Anhydrous solvents (*N*, *N*-dimethylformamide (DMF) and pyridine) were purchased from Acros Organics and used without further purification. Dendritic polyglycerol (dPG) with a degree of branching of 60%, M_n = 7.3 kDa, and M_w = 10.3 kDa (PDI = 1.4), was obtained from nanopartica. Methanesulfonyl chloride (MsCl), sodium azide, and 4-nitrophenol chloroformate were purchased from Sigma Aldrich. Sulfur trioxide pyridine complex was purchased from Alfa Aesar, tris(2-carboxyethyl)phosphine (TCEP) from Roth, propargyl-PEG1-SS-alcohol from Broadpharm, Boc-β-Ala-OSu (Boc-β-alanine N-hydroxysuccinimide ester) from Bachem, mal-dPEG(4)-NHS from Celares, and MMAE·TFA from Levena Biopharma.

Conjugation reactions were performed in Eppendorf tubes which were shaken with 750 rpm in a BioShake iQ from Quantifoil Instruments GmbH.

Purification of polymeric structures was performed by ultrafiltration or dialysis using regenerated cellulose, while the small molecular weight compounds were purified by column chromatography using a CombiFlash Rf + from Teledyne ISCO and pre-packed silica columns.

2.2. Characterization

^{1}H NMR and ^{13}C NMR were recorded on a Bruker AVANCE III 700 spectrometer (700 MHz for ^{1}H and 176 MHz for ^{13}C) at 25 °C. NMR chemical shifts were reported as δ values in ppm and were referenced to the indicated deuterated solvents methanol (MeOH-d4, ^{1}H: 3.31 ppm, ^{13}C: 49.0 ppm), water (D_2O, ^{1}H: 4.79 ppm) and chloroform ($CDCl_3$, ^{1}H: 7.26 ppm, ^{13}C: 77.16 ppm). NMR data are reported as follows: chemical shift, multiplicity (s = singlet, d = doublet, t = triplet, m = multiplet), coupling constant in Hertz (Hz), integration. Multiplets (m) were reported over the range (ppm) at which they appeared at the indicated field strength. Elemental analysis (EA) was conducted using a vario EL element analyzer. Both the calculated and the found amounts for the elements carbon (C), nitrogen (N), hydrogen (H), and sulfur (S) were reported. Infrared (IR) spectra were obtained using a JASCO FTIR-4100 spectrophotometer, which was equipped with a PIKE diamond (ATR method, attenuated total reflection). The vibration bands were reported as ν values in cm^{-1}. Electrospray ionization (ESI) mass spectra (MS) were recorded on an Agilent 6210 TOF LC/MS System.

2.3. Functionalization of dPG

To obtain dPGS-based nanocarriers suitable for further chemical conjugation, dPG-OH was functionalized as previously reported [9,16]. Non-sulfated derivatives served as controls. Briefly, azide-functionalized dPG (dPG-N_3) was obtained by partial mesylation with MsCl in pyridine and subsequent azidation with NaN_3 in DMF. The residual hydroxy groups were sulfated with sulfur trioxide-pyridine complex. The amount of azide and sulfate groups was determined by EA to be 13% and 87%, respectively. Finally, the azide groups were reduced to amine groups with TCEP under aqueous conditions. The success of reaction was confirmed by IR spectroscopy showing finally no band at 2100 cm^{-1} anymore. More physicochemical data of the polymeric carriers can be found in Table S1.

2.4. Synthesis of propargyl-SS-MMAE

Propargyl-SS-nitrophenol. A solution of propargyl-PEG1-SS-alcohol (50.9 mg, 265 µmol) in acetonitrile (MeCN, 2 mL) was cooled to 0 °C with an ice bath. Triethylamine (73.5 µL, 530 µmol) and 4-nitrophenylchloroformate (80.4 mg, 399 µmol) were added, and the reaction mixture was stirred for 24 h at room temperature. The solvent was removed under reduced pressure, and the crude product was purified by automated column chromatography (24 g column, cyclohexane/EtOAc). The product was obtained as a yellow oil (72.8 mg, 77%). NMR spectra are shown in Fig. S1-S4. ^{1}H NMR (700 MHz, $CDCl_3$) δ = 8.29–8.27 (m, 2H, H-2 and H-2′), 7.40–7.38 (m, 2H, H-3 and H-3′), 4.56 (t, J = 6.6 Hz, 2H, H-6), 4.20 (d, J = 2.4 Hz, 2H, H-10), 3.80 (t, J = 6.3 Hz, 2H, H-9), 3.05 (t, J = 6.6 Hz, 2H, H-7), 2.96 (t, J = 6.3 Hz, 2H, H-8), 2.46 (t, J = 2.4 Hz, 1H, H-12) ppm. ^{13}C NMR (176 MHz,

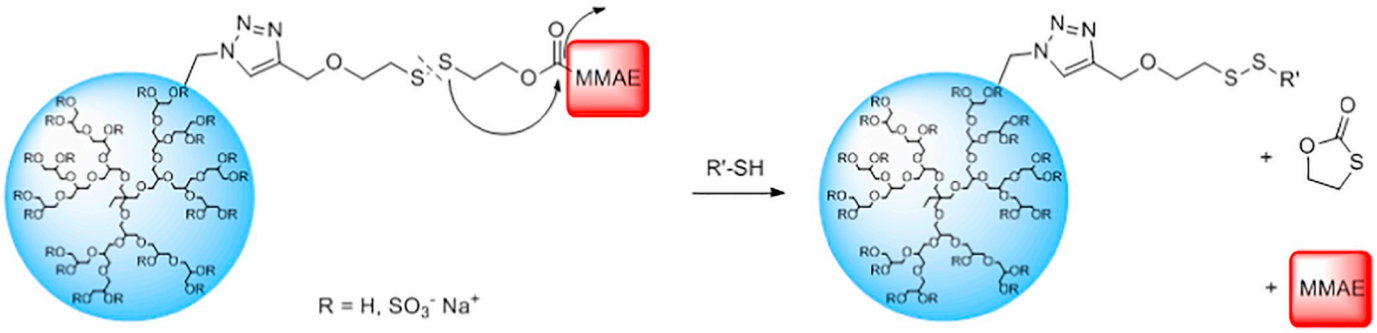

Fig. 1. Drug release from dPG-SS-MMAE (R = H) and dPGS-SS-MMAE (R = SO_3^- Na^+) under reductive conditions. After disulfide cleavage and self-immolation, the drug is released without a portion of the linker.

$CDCl_3$) δ = 155.5 (C-4), 152.4 (C-5), 145.6 (C-1), 125.5 (C-2), 121.9 (C-3), 79.4 (C-11), 75.0 (C-12), 68.1 (C-9), 67.0 (C-6), 58.4 (C-10), 38.8 (C-8), 36.8 (C-7) ppm. MS (ESI-TOF): calcd. for $C_{14}H_{15}N_1O_6S_2$ 380.0233 $[M + Na]^+$, 395.9972 $[M + K]^+$; found 380.0275 $[M + Na]^+$, 396.0034 $[M + K]^+$. IR (ATR): υ = 3446, 3288 (C≡C), 2918, 2112, 1764, 1616, 1594, 1522, 1492, 1457, 1345, 1251, 1209, 1164, 1078, 1042, 1011, 982, 931, 858, 771, 754 cm^{-1}.

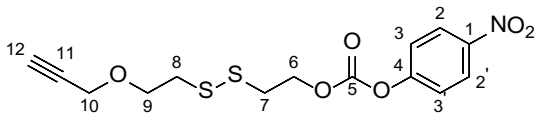

Propargyl-SS-MMAE. MMAE·TFA (50.0 mg, 60.1 μmol) and propargyl-SS-nitrophenol (43.0 mg, 120 μmol) were dissolved in DCM (1 mL). Triethylamine (42.0 μL, 303 μmol) and HOBt (16.1 mg, 119 μmol) were added, and the reaction mixture was stirred for 3 d at room temperature. The solvent was removed under reduced pressure, and the crude product was purified by automated column chromatography (40 g column, DCM/MeOH). The product was obtained as a colorless solid (44.6 mg, 79%). NMR spectrum is shown in Fig. S6. MS (ESI-TOF): calcd. for $C_{47}H_{77}N_5O_{11}S_2$ 958.5004 $[M + Na]^+$, 974.4743 $[M + K]^+$; found 958.5015 $[M + Na]^+$, 974.4745 $[M + K]^+$.

2.5. Synthesis of mal-dPEG(4)-MMAE

Boc-β-Ala-MMAE. MMAE·TFA (29.9 mg, 35.9 μmol) was dissolved in dry DCM (1 mL). DIPEA (30.7 μL, 179 μmol) and Boc-β-Ala-OSu (15.5 mg, 54.1 μmol) were added, and the reaction mixture was stirred for 1.5 d at room temperature. Again, Boc-β-Ala-OSu (15.6 mg, 54.5 μmol) was added and the mixture was stirred for further 1.5 d. The solvent was removed under reduced pressure and the crude product was purified by automated column chromatography (24 g column, DCM/MeOH) to afford the desired product (30.1 mg, 94%). NMR spectrum is shown in Fig. S7. MS (ESI-TOF): calcd. for $C_{47}H_{80}N_6O_{10}$ 889.6009 $[M + H]^+$, 911.5828 $[M + Na]^+$, 927.5568 $[M + K]^+$; found 889.6038 $[M + H]^+$, 911.5871 $[M + Na]^+$, 927.5595 $[M + K]^+$.

β-Ala-MMAE. Boc-β-Ala-MMAE (30.1 mg, 33.9 μmol) was dissolved in DCM (1.3 mL). TFA (130 μL, 1.69 mmol) was added and the reaction mixture was stirred for 2 h at room temperature. The crude product was concentrated in vacuo and the TFA was co-evaporated several times with DCM to afford the desired product (28.3 mg, quant.). NMR spectrum is shown in Fig. S8. MS (ESI-TOF): calcd. for $C_{42}H_{72}N_6O_8$ 789.5484 $[M + H]^+$, 811.5304 $[M + Na]^+$, 827.5043 $[M + K]^+$; found 789.5538 $[M + H]^+$, 811.5345 $[M + Na]^+$, 827.5079 $[M + K]^+$.

Mal-dPEG(4)-MMAE. β-Ala-MMAE (15.1 mg, 19.2 μmol) was dissolved in DCM (0.5 mL). DIPEA (16.4 μL, 95.8 μmol) and mal-dPEG(4)-NHS (19.7 mg, 38.4 μmol) were added, and the reaction mixture was stirred for 3 d at room temperature. The solvent was removed under reduced pressure and the crude product was purified by automated column chromatography (24 g column, DCM/MeOH) to afford the desired product (20.3 mg, 89%). NMR spectrum is shown in Fig. S9. MS (ESI-TOF): calcd. for $C_{60}H_{98}N_8O_{16}$ 1209.6993 $[M + Na]^+$, 616.3443 $[M + 2Na]^{2+}$; found 1209.6967 $[M + Na]^+$, 616.3435 $[M + 2Na]^{2+}$.

2.6. Synthesis of PDCs

dPGS-SS-$MMAE_1$. To dPGS-N_3 (50.0 mg, 2.25 μmol) in an Eppendorf tube were added propargyl-SS-MMAE (150 μL of a stock solution of 13.8 mg in 655 μL MeOH, 3.38 μmol), $CuSO_4{\cdot}5H_2O$ (250 μL of a stock solution of 5.961 mg in 2.65 mL PBS, 2.25 μmol, 5 mol% per azide group), and sodium ascorbate (250 μL of a stock solution of 10.864 mg in 1.22 mL PBS, 11.3 μmol, 25 mol% per azide group). The solvent mixture was equilibrated to a MeOH/PBS ratio of 1:1 and the reaction was left to proceed at 40 °C for 3 d. The solvent was removed under reduced pressure, and the crude product was purified by dialysis (MWCO 2000) in ethylenediaminetetraacetic acid (EDTA)-disodium solution (10 g/L), saturated NaCl solution, water, and water/MeOH 1:1 in succession. After concentration in vacuo and lyophilization, the product was obtained as a colorless solid (44.4 mg, 85%).

dPGS-SS-$MMAE_5$. dPGS-N_3 and propargyl-SS-MMAE (500 μL of a stock solution, 11.2 μmol) were reacted and the crude product was purified as described for dPGS-SS-$MMAE_1$. Lyophilization afforded the product as a colorless solid (46.4 mg, 77%).

dPG-SS-$MMAE_1$. To dPG-N_3 (20.0 mg, 1.90 μmol) in an Eppendorf tube were added propargyl-SS-MMAE (60 μL of a stock solution of 20.6 mg in 462 μL MeOH, 2.86 μmol), $CuSO_4{\cdot}5H_2O$ (100 μL of a stock solution of 5.27 mg in 1.10 mL PBS, 1.91 μmol, 5 mol% per azide group), and sodium ascorbate (100 μL of a stock solution of 6.95 mg in 369 μL PBS, 9.49 μmol, 25 mol% per azide group). The solvent mixture was equilibrated to a MeOH/PBS ratio of 1:1 and the reaction was left to proceed at 40 °C for 3 d. The solvent was removed under reduced pressure, and the crude product was purified by dialysis (MWCO 1000) in EDTA-disodium solution (10 g/L), water, and water/MeOH 1:1 in succession. After concentration in vacuo and lyophilization, the product was obtained as a colorless solid (15.9 mg, 73%).

dPG-SS-$MMAE_5$. dPG-N_3 and propargyl-SS-MMAE (200 μL stock solution, 9.53 μmol) were reacted and the crude product was purified as described for dPG-SS-$MMAE_1$. Lyophilization afforded the product as a colorless solid (11.9 mg, 41%).

dPGS-MMAE. To dPGS-NH_2 (10.1 mg, 465 nmol) in an Eppendorf tube were added iminothiolane hydrochloride (192 μL of a stock solution of 2.5 mg in 1.5 mL water, 320 μg, 2.33 μmol) and DIPEA (55.7 μL of a stock solution of 5 μL in 500 μL DMF, 3.25 μmol) as well as DMF and water up to a final volume of 400 μL of a 1:1 mixture. The reaction mixture was shaken in a bioshaker for 15 min at 25 °C and 750 rpm. Mal-dPEG(4)-MMAE (2.76 mg, 2.32 μmol) was added, and the reaction mixture was shaken for further 24 h at 25 °C and 750 rpm. The solvent was removed under reduced pressure, and the crude product was purified by dialysis (Slide-A-Lyzer Dialysis Cassette, MWCO 7000) stepwise in saturated NaCl solution, water, and water/MeOH 1:1. After concentration in vacuo and lyophilization, the product was obtained as a colorless solid (8.2 mg, 62%). NMR spectrum is shown in Fig. S10.

2.7. Dye labeling

For in vitro studies, dPG-SS-$MMAE_1$ and dPGS-SS-$MMAE_1$ conjugates were labeled with an indocarbocyanine (ICC) dye via alkyne-azide cycloaddition reaction according to Licha et al. [17].

2.8. Determination of drug-to-carrier ratios by analytical HPLC

Analytical high-performance liquid chromatography (HPLC) was performed using a Smartline system from Knauer, equipped with a pump 1000, degasser, autosampler 3950, and variable wavelength UV detector 2500. The stationary phase was a pre-packed column (125 × 4.6 mm) with RP-18 material (RSC-Gel, C18ec, 5 μm) from R. Sauerbrey Chromatographie. UV detection was performed at 220 nm. The flow was 1.0 mL·min^{-1}. Eluent was a degassed MeCN-water mixture with 40% MeCN (vol-%, isocratic method). Ammonium formiate (AFo) was used as modifier (10 mM effective concentration, pH 7). The temperature was 60 °C.

1 mg of each conjugate was dissolved in a solution of PBS (pH 7.4, 200 μL) with dithiothreitol (DTT, 30 mM) and EDTA (2 mM). The mixture was shaken for 3 d at 37 °C and subsequently lyophilized. The solid was suspended in acetonitrile (1 mL) and mixed strongly. After centrifugation, the supernatant was concentrated in vacuo. The resulting residue was dissolved in 500 μL of the 40% MeCN (10 mM AFo) solution used for HPLC. 10 μL of each solution were analyzed three times by HPLC. The mean of the integrals for each conjugate was compared with a calibration curve of free MMAE, giving the amount of

the released MMAE.

2.9. Stability in cell culture medium and proof of concept

A solution of dPGS-SS-MMAE$_1$ in RPMI cell culture medium (10 μM) was stored for 2 d at 37 °C. A solution of dPGS-SS-MMAE$_1$ in RPMI supplemented with DTT (30 mM) and EDTA (2 mM) served as a control. After lyophilization, the solids were suspended in acetonitrile (3 mL) and mixed strongly. After centrifugation, the supernatants were concentrated in vacuo. The residues were dissolved in MeOH and analyzed by mass spectrometry.

2.10. Cell culture

The human cancer cell lines A549 (lung carcinoma), HeLa (cervix carcinoma), MCF-7 (breast adenocarcinoma), and Caco-2 (colon adenocarcinoma) were obtained from DSMZ, Braunschweig. A549 cells were cultured in DMEM and the other three cell lines in RPMI medium, both media supplemented with 10% (vol-%) fetal bovine serum (FBS) and 1% (vol-%) penicillin/streptomycin (P/S). Monolayers of cells were cultured in a humidified atmosphere containing 5% CO_2 at 37 °C. Subcultivation was done twice a week using trypsin/EDTA. Cells were counted by Luna automated cell counter, after treatment with Trypan Blue (Bio Whittaker).

2.11. Real-time cell analysis

For real-time cell analysis (RTCA), A549 cells were seeded in a 96-well *E*-plate at a cell density of 4×10^3 cells/well. After 3 d, the cell culture medium was carefully exchanged, and different samples were added. dPGS-SS-MMAE$_1$, dPG-SS-MMAE$_1$, and MMAE·TFA were added to a final concentration of 100 nM. Non-treated and sodium dodecyl sulfate (SDS, 100 μg/mL) treated cells served as controls, and medium alone (without any cells) was used for baseline correction.

2.12. Cell proliferation and cytotoxicity assay

In vitro cytotoxicity of the PDCs was evaluated using cell counting kit 8 (CCK-8, Dojindo Molecular Technologies, Inc.). 4×10^3 cells/well were seeded in 96-well plates. After 24 h, serial dilutions of the conjugates and control samples were incubated for 48 h at 37 °C. The CCK-8 dye was incubated for 2 h. The absorbance was measured at 450 nm using a Tecan Infinite® 200PRO plate reader, which was equipped with a Tecan i-control software. The values were normalized to the non-treated control. In each experiment SDS served as a control that immediately caused cell death giving 0% cell viability. Neither the 100% nor the 0% controls are shown in the diagrams.

2.13. Flow cytometry

For cellular uptake studies, cells were seeded at a density of 5×10^5 cells/well in 24-well plates and cultured at 37 °C for 4 h. ICC-labeled PDCs were added and incubated for 18 h at a final dye concentration of 1 μM. Cells were washed three times with PBS, detached with trypsin, centrifuged, suspended in PBS (200 μL), and finally analyzed using a BD Accuri C6 flow cytometer (BD Biosciences). At least 10,000 cells were analyzed for each sample, with excitation at 488 and 640 nm and detection at FL2 585/40 nm. Data analysis was performed with FlowJo Data Analysis Software. By gating we excluded successively cell debris (SSC-A against FSC-A) and doubletts (FSC-H against FSC-A). The histograms were finally plotted as the counts against the fluorescence intensity in FL2 including the geometric means.

2.14. Confocal laser scanning microscopy

The cellular uptake of the ICC-labeled PDCs was additionally studied with confocal laser scanning microscopy (CLSM). Therefore, cells were seeded in 8-well Ibidi slides at a density of 1.2×10^4 cells/well and cultured at 37 °C for 4 h. Cells were then incubated with ICC-labeled conjugates for 18 h at a final dye concentration of 1 μM. The nuclei were stained with Hoechst 44432 (Invitrogen) and the acidic compartments were stained with LysoTracker® Green DND-26 (Life technologies). Finally, the cellular uptake was studied with CLSM using a Leica TCS SP8 microscope and a 63× oil immersion objective. Analysis of the images was performed with the Leica Application Suite X (LAS X) software.

2.15. Maximum tolerated dose study

For maximum tolerated dose (MTD) studies, Balb/c mice were administered with a single dose of dPGS-SS-MMAE$_5$ via tail vein injection. PBS and free MMAE were used as controls. The body weight was monitored daily for 10 days. The MTD is defined as the highest dose that does not cause unacceptable toxicity like death, over 15% body weight loss, or other remarkable changes in the general appearance of the mice within the experiment period.

3. Results

3.1. Synthesis of cleavable conjugates

To obtain cleavable PDCs (Fig. 2), a linker strategy was used similar to that described by Batisse et al. [13]. This linker strategy involves a chemical structure, which liberates the parent MMAE moiety due to a traceless spontaneous decomposition after reductive cleavage. In the present work, propargylglycol-SS-glycol and 4-nitrophenol chloroformate were reacted to get a reductively cleavable disulfide linker that was further reacted with MMAE under formation of a carbamate connection. 1.5 and 5 equivalents of this MMAE-linker moiety were subsequently reacted with dPGS-N_3 under Cu-catalyzed alkyne-azide cycloaddition reaction to get the desired dPGS-SS-MMAE conjugates. The corresponding non-sulfated dPG-SS-MMAE conjugates were synthesized as controls.

The amount of drug molecules per polymer was determined by HPLC after in situ cleavage of the PDCs using the reducing agent DTT. This indirect method was developed to overcome the lack of a robust direct analytical method to quantify MMAE relative to the dPG carrier backbone. NMR spectroscopy, which is usually used, could not be applied as the sensitivity is too low to reliably quantify signals derived from the MMAE molecule beside the huge polymer backbone, and these were distributed over the whole spectrum and coincided with the polymer peaks. Quantifying the measured HPLC peak areas of MMAE derived from cleaved conjugates in relation to a calibration curve of different amounts of free MMAE, the average drug-to-carrier ratios were calculated to be approximately 1 and 5, respectively, for the two envisaged conjugate compositions.

Beside the cleavable dPGS-SS-MMAE conjugates, a non-cleavable counterpart (dPGS-MMAE) was synthesized additionally to further elucidate the impact of the drug release on cell toxicity relative to stable conjugates, thereby addressing the question whether drug liberation is advantageous or even crucial to make the conjugates acting as potent anticancer agents. We wanted to introduce a short but flexible PEG spacer in dPGS-MMAE to enable tubulin binding. In first attempts, we tried to couple the commercial bifunctional linker maleimido tetraethylene glycol NHS ester (mal-dPEG(4)-NHS) directly with MMAE, giving low conversion and yields unfortunately. This was probably due to the lower reactivity of the secondary amino group in MMAE and/or steric hindrance due to adjacent bulky alkyl groups. Therefore, the secondary amine was prolonged with a small spacer based on β-alanine to introduce a primary amine that was more reactive and sterically not hindered. As opposed to the PEG spacer mentioned above, modification with β-alanine worked satisfactorily. Accordingly, the successfully

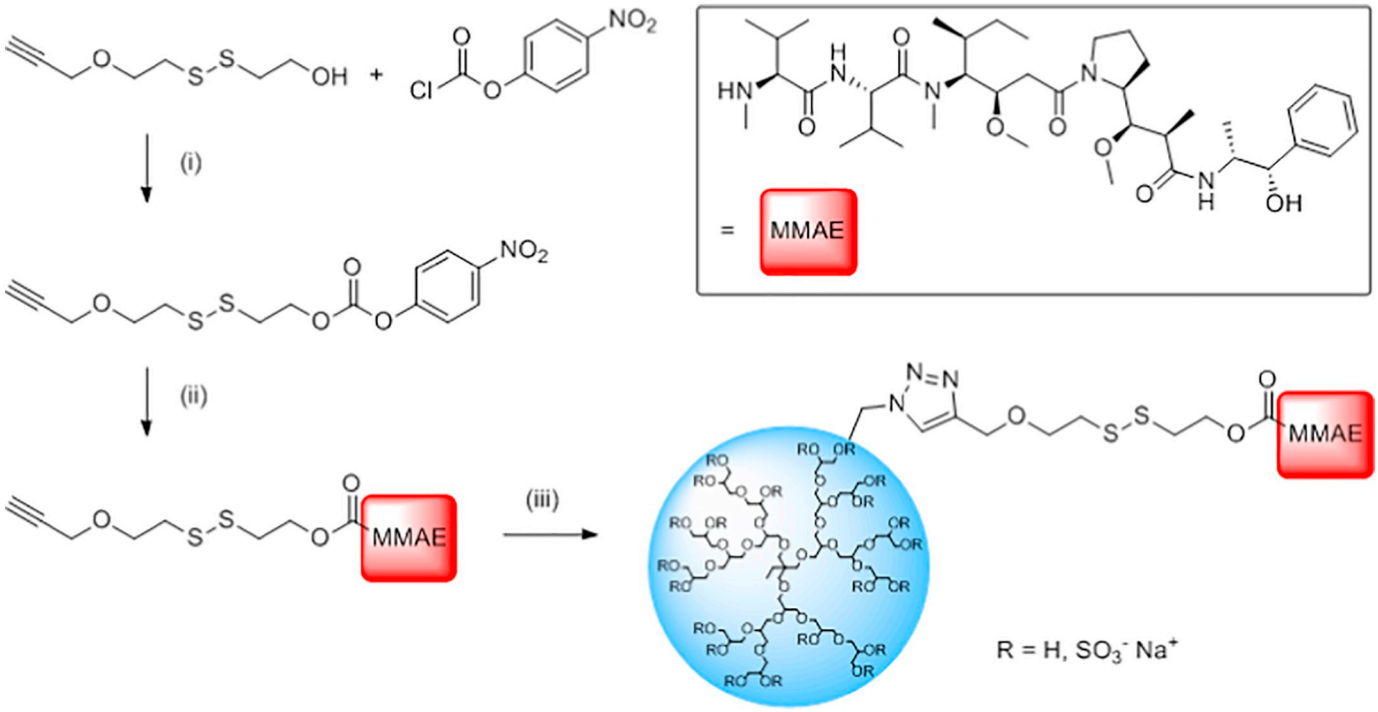

Fig. 2. Synthetic route for cleavable dPG- and dPGS-SS-MMAE conjugates. Conditions: (i) NEt_3, MeCN, 24 h, 0 °C ➔ r.t., 77%; (ii) MMAE·TFA, HOBt, NEt_3, DCM, 3 d, r.t., 79%; (iii) dPG-N_3 or dPGS-N_3, $CuSO_4{\cdot}5H_2O$, sodium ascorbate, MeOH/PBS, 3 d, 40 °C.

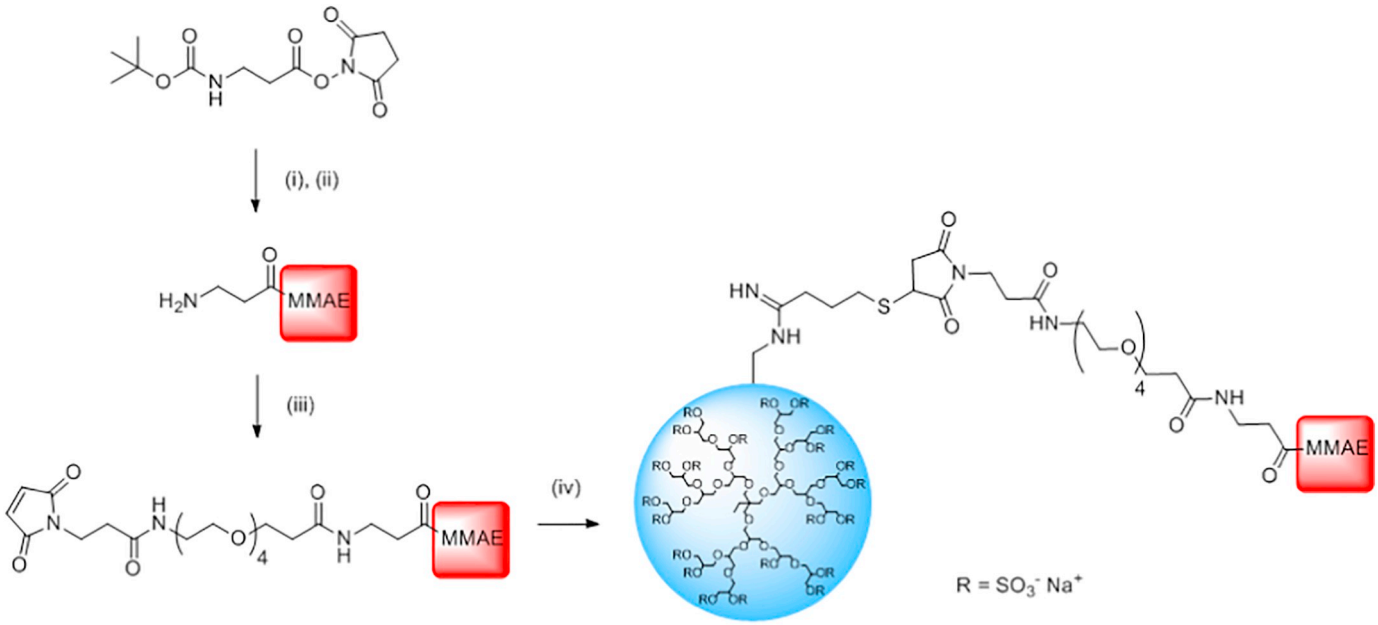

Fig. 3. Synthetic route for non-cleavable dPGS-MMAE conjugates. Conditions: (i) MMAE·TFA, DIPEA, DCM, 3 d, r.t., 94%; (ii) TFA, DCM, 2 h, r.t., quant.; (iii) mal-dPEG(4)-NHS, DIPEA, DCM, 3 d, r.t., 89%; (iv) dPGS-N_3, iminothiolane hydrochloride, DIPEA, DMF/H_2O, 24 h, r.t.

established synthesis of the non-cleavable dPGS-MMAE conjugate based on this approach is shown in Fig. 3. For the last reaction, 5 equivalents of mal-dPEG(4)-MMAE were used to yield a non-cleavable control conjugate. The NMR spectrum of dPGS-MMAE (Fig. S10) shows the dPGS and MMAE signals, but a quantitative analysis by NMR was not possible due to the reasons mentioned for the cleavable conjugates. Therefore, we assumed a drug-to-polymer ratio between 1 and 5, allowing at least a qualitative use in the in vitro studies.

In total, one non-cleavable and four cleavable PDCs were synthesized and analyzed in vitro. They will be abbreviated with dPGS-MMAE, dPGS-SS-$MMAE_1$, dPGS-SS-$MMAE_5$, dPG-SS-$MMAE_1$, and dPG-SS-$MMAE_5$.

3.2. Stability under physiological conditions and proof of concept

The stability of the cleavable PDCs under physiological conditions was confirmed by mass spectrometry. Accordingly, dPGS-SS-$MMAE_1$ was incubated in cell culture medium for 2 d at 37 °C. In a second vial, which served as a control, DTT (30 mM) was supplemented to chemically cleave the conjugate. Both mixtures were lyophilized after 2 d.

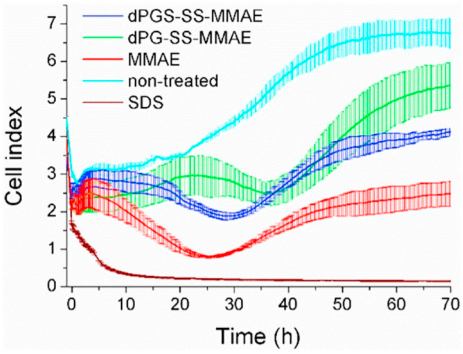

Fig. 4. RTCA of the proliferation of A549 cells treated with dPGS-SS-MMAE$_1$, dPG-SS-MMAE$_1$, and MMAE after 72 h. Non-treated cells and SDS treated cells served as controls. The means ± SD of two data points were plotted for each timepoint.

Potential free drug was extracted and finally analyzed by mass spectrometry. The peak of free MMAE was detected after chemical cleavage (Fig. S11, left), which showed that MMAE was liberated without a portion of the linker in the presence of a reducing agent. On the contrary, the peak was not detected after leaving the PDC in pure cell culture medium (Fig. S11, right) which indicates the conjugate's stability under physiological conditions.

3.3. Real-time cell analysis

We studied the effect of linker cleavage and drug release kinetics on cell viability and proliferation by applying the method of RTCA (Fig. 4). Cells were cultured for 72 h until a linear increase of the cell index was observed, before dPGS-SS-MMAE$_1$, dPG-SS-MMAE$_1$, and MMAE were added at a concentration of 100 nM. Non-treated and SDS treated cells served as controls. Non-treated cells expectedly showed an increase in cell proliferation over time, whereas the cell index decreased immediately after addition of SDS. For the three other samples the cell index further increased in the beginning, then moved into a delayed decreasing slope, and finally re-increased indicating a recovery of the surviving cells. Free MMAE showed a faster effect than the conjugates as the cell index minimum for MMAE was reached after 25 h, for dPGS-SS-MMAE after 28 h, and for dPG-SS-MMAE after 36 h. This finding correlates well with the expectation that the cleavage process in the PDCs needed to occur first, thus generating a certain delay in toxic response. The much later toxic response of the non-sulfated conjugate compared to the sulfated one might be attributed to the less cellular uptake as expected from the literature [17–21]. This was confirmed by cellular uptake studies, which will be described later.

3.4. Cell proliferation and cytotoxicity assay

To study the applicability of the synthesized PDCs against a variety of cancer types, we chose four different human cancer cell lines that belong to the most common cancer types. The cell viability was examined by the CCK-8 proliferation and cytotoxicity assay following 48 h incubation of A549 (lung carcinoma), HeLa (cervix carcinoma), MCF-7 (breast adenocarcinoma), and Caco-2 (colon adenocarcinoma) cells with the PDCs as well as free MMAE (Fig. 5). Non-treated cells served as the control that was set to 100% cell viability (not shown in the diagrams).

On A549 and HeLa cells (Fig. 5, top), the conjugates were cytotoxic in the nanomolar range with the sulfated conjugates being more effective than the non-sulfated ones. In general, the conjugates were less cytotoxic than the parent drug, which is in agreement with literature [9,22] and appropriate, since MMAE is a highly potent cytostatic drug that also causes unwanted systemic side effects. With our approach, the drug should be made more specific, making it applicable as a drug with low systemic off-target effects. The IC_{50} values were determined with respect to the conjugate's concentration as well as to the drug's concentration (Table 1). The higher loaded PDCs were 2- to 5-fold more cytotoxic compared to their analogs with only one drug molecule per polymer.

In contrast, MCF-7 and Caco-2 cells (Fig. 5, bottom) were hardly affected by treatment with the conjugates and the drug itself up to a concentration of 100 nM. Therefore, in vitro studies with these cell lines and treatment of breast and colorectal cancer with the PDCs described here were not further pursued.

A reason for the different observations between the cell lines could be that A549 and HeLa cells proliferate faster compared to MCF-7 and Caco-2 cells. By acting as a tubulin inhibitor, MMAE prevents cell division, directly affecting the proliferation rate. Thus, the cytotoxic effect can be more clearly seen for A459 and HeLa cells.

As discussed above, non-cleavable dPGS-MMAE conjugates were synthesized to study whether the cleavability of such conjugates and the release of free drug is advantageous or even crucial to make these conjugates cytotoxic. dPGS-MMAE was tested on A549 and HeLa cells but, in contrast to the cleavable conjugates, no cytotoxic effects were observed up to a concentration of 100 nM (Fig. S12). Comparison of the cytotoxicity effects of cleavable with non-cleavable PDCs led to the conclusion that the triggered release is necessary for the application as anticancer agent. This finding was in good accordance with the literature [23].

3.5. Cellular uptake studies

The cellular uptake of ICC-labeled dPGS-SS-MMAE$_1$ and dPG-SS-MMAE$_1$, respectively, was studied by flow cytometry and by CLSM using A549 and HeLa cells. In general, in both experiments and on both cell lines, the sulfated conjugate showed higher cellular uptake than the non-sulfated one as expected from the literature [17–21]. In the flow cytometry experiment (Fig. 6), cells treated with the sulfated conjugate gave higher fluorescence intensities than with the non-sulfated one, indicating that the polyanionic surface led to better internalization. To further analyze cell binding and the uptake mechanism, we repeated the experiment with incubation for 1 h at 4 °C and at 37 °C for comparison. Fig. S13 shows higher fluorescence intensities at 37 °C than at 4 °C for both the sulfated as well as the non-sulfated PDCs treated cells indicating that the compounds are mainly taken up by an energy driven pathway such as endocytosis. Comparing the fluorescence signals from dPG and dPGS at 4 °C we see a clearly better binding of dPGS to the cell surface. This could also explain the more pronounced uptake of the charged compound dPGS.

To gain more precise information on the subcellular localization of the conjugates, the cellular uptake was further studied by CLSM. A549 and HeLa cells were incubated with the ICC-labeled conjugates (red color in the CLSM images) for 18 h, washed and stained with Hoechst (nucleus, blue) and LysoTracker (acidic compartments like endosomes and lysosomes, green). Since both cell lines gave similar results, only the images from the A549 cells are shown here exemplarily (Fig. 7). On both cell lines, cellular uptake for the sulfated PDCs was already observed after 4 h (not shown), which increased over time, while cellular uptake of non-sulfated PDCs could hardly be observed even after 18 h, which correlated well with the literature [17–21], and underscored the need of the sulfate groups on the surface for improved cellular uptake. On both cell lines, the sulfated conjugate seemed to be equally distributed within the cell around the nucleus, being associated with acidic compartments, since the fluorescence of the ICC dye was only co-localized with the fluorescence of the LysoTracker. This co-localization

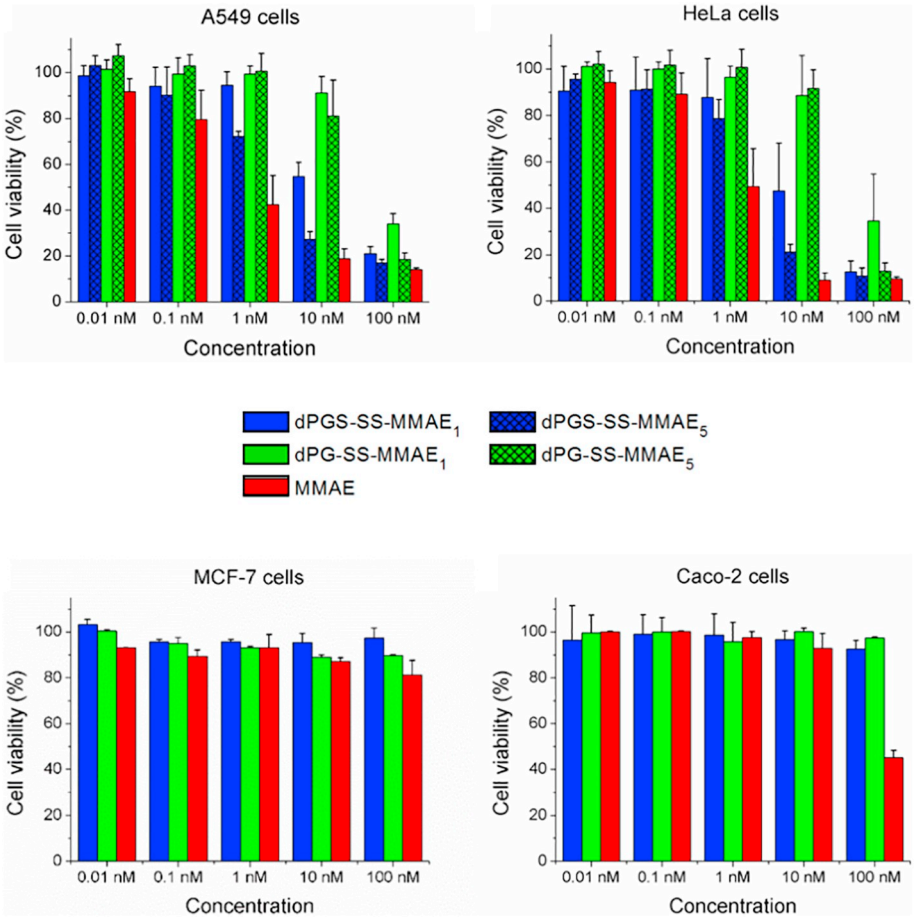

Fig. 5. Viability of different human cancer cell lines following 48 h incubation of cleavable conjugates as well as the free drug ($n \geq 2$). Data are presented as mean ± SD.

Table 1
IC_{50} values of MMAE and the conjugates in A549 and HeLa cells ($n \geq 3$). The values were determined firstly based on the conjugate concentration and secondly on the MMAE concentration.

Sample	IC_{50} values in A549 cells based on the concentration of		IC_{50} values in HeLa cells based on the concentration of	
	the conjugate	or MMAE	the conjugate	or MMAE
MMAE	0.53 nM	0.53 nM	0.97 nM	0.97 nM
dPGS-SS-$MMAE_1$	8.8 nM	8.8 nM	9.0 nM	9.0 nM
dPGS-SS-$MMAE_5$	1.8 nM	8.9 nM	2.6 nM	13 nM
dPG-SS-$MMAE_1$	42 nM	42 nM	50 nM	50 nM
dPG-SS-$MMAE_5$	17 nM	88 nM	27 nM	134 nM

demonstrates that the conjugates were mainly transported to the lysosomes indicating endocytosis which is in line with the flow cytometry results. In summary, from flow cytometry and confocal microscopy experiments, we concluded that the cellular uptake mainly occurs by endocytic pathways.

3.6. Maximum tolerated dose study

The most potential conjugate, namely, dPGS-SS-$MMAE_5$ was chosen for further in vivo studies. While the conjugate should cause cytotoxic effects on tumor cells, it should not harm healthy tissue and animals. To obtain insight into the systemic tolerability of the conjugate in living organisms, a study to determine the maximal tolerated dose was conducted in Balb/c mice. These data will serve as a basis to obtain treatment dose regimens and determine the therapeutic window for the desired disease model (such as tumor-bearing mice). Therefore, the weight loss of mice was studied after treatment with different concentrations of dPGS-SS-$MMAE_5$ as well as with free MMAE and PBS as controls (Fig. 8). Single doses were administered via tail vein injection. While the free drug caused continuous weight loss with start of treatment, indicating acute toxicity to the organism, the conjugate was well tolerated, even at a MMAE concentration that was 30-fold above that of the toxic MMAE alone.

4. Conclusion

Here we presented the synthesis and biological evaluation of PDCs made of dPG as the carrier and the highly potent drug MMAE. We

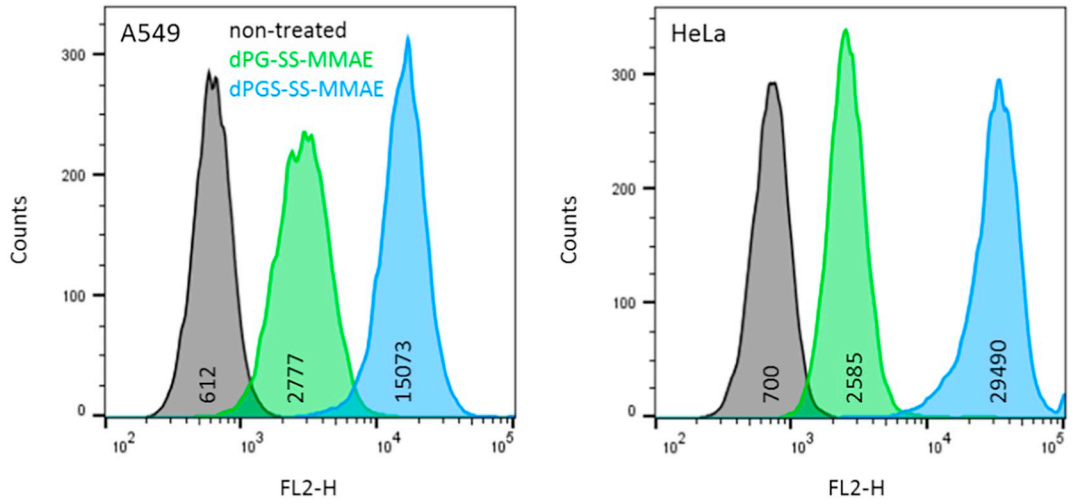

Fig. 6. Flow cytometry studies of A549 and HeLa cells following 18 h incubation with ICC-labeled dPGS-SS-MMAE$_1$ and dPG-SS-MMAE$_1$. Non-treated cells served as the control. The numbers represent the geometric means of the fluorescence intensities.

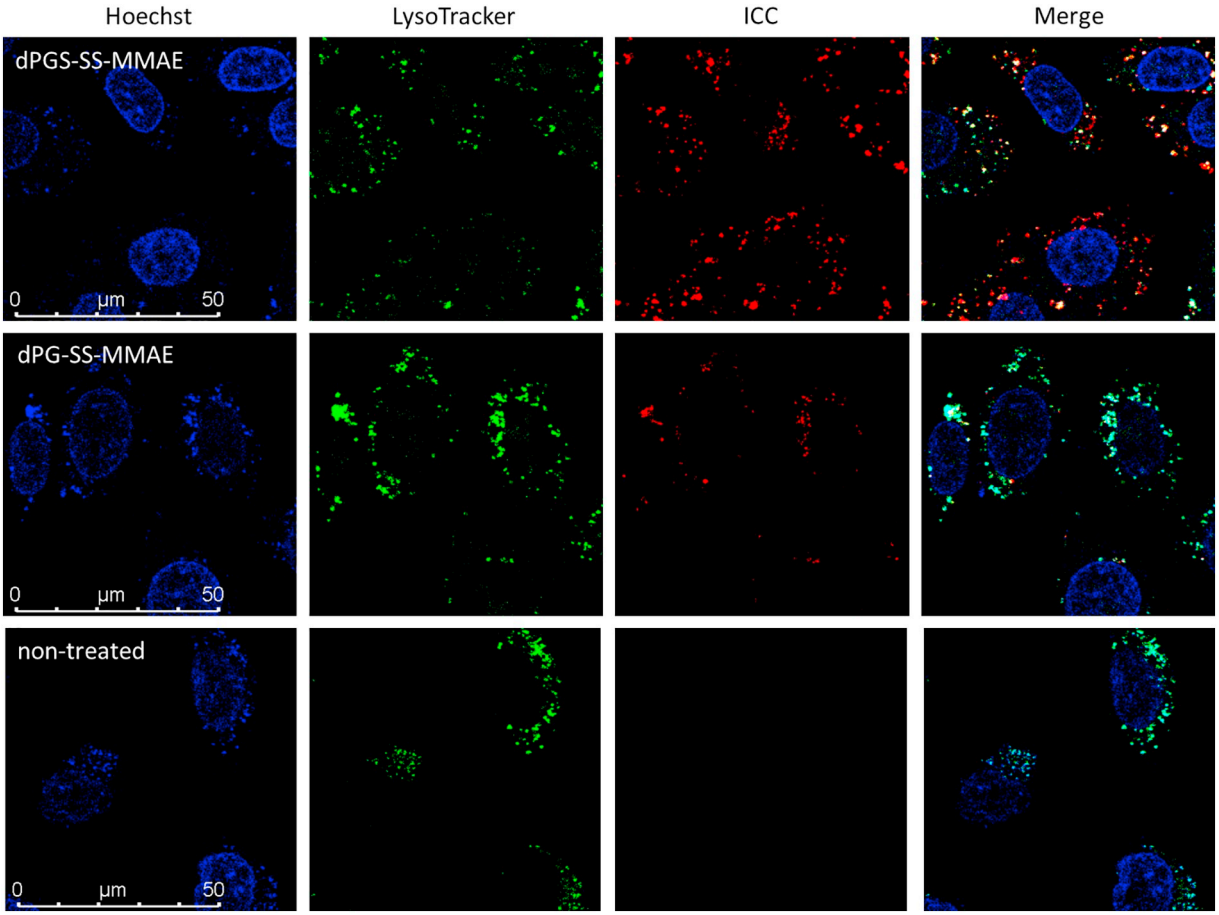

Fig. 7. CLSM images of A549 cells following 18 h incubation with ICC-labeled dPGS-SS-MMAE$_1$, and dPG-SS-MMAE$_1$. The final ICC concentration was 1 µM. Non-treated cells served as a control. In each row, the images show cell nuclei stained with Hoechst (blue, excitation: 405 nm, detection: 495–577 nm), acidic compartments stained with LysoTracker (green, excitation: 488 nm, detection: 495–577 nm), ICC fluorescence (red, excitation: 561 nm, detection: 584–748 nm), and overlays of the three images (from left to right). The magnification is always the same and the corresponding scale bars correspond to 100 µm.

showed that sulfation of the carrier as well as the cleavable linker is necessary for improved cellular uptake and cell toxicity, respectively.

Since the reductively cleavable dPGS-SS-MMAE conjugates showed promising results with the human cancer cell lines A549 and HeLa in vitro, and we did not observe systemic in vivo toxicity, these conjugates could be potential candidates for further treatment studies that are currently planned.

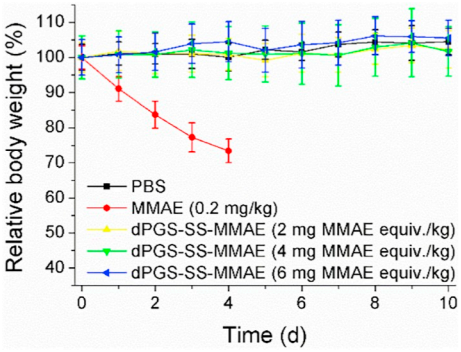

Fig. 8. MTD assays of dPGS-SS-MMAE$_5$ in Balb/c mice (n = 5). Data are presented as mean ± SD.

Declarations of interest

None.

Funding

This work was supported by the Helmholtz Virtual Institute on "Multifunctional Biomaterials for Medicine", the German Science Foundation (DFG) [392192146] and the National Natural Science Foundation of China [51761135117].

Acknowledgements

We are grateful to Paul Hillmann and Elisa Quaas for their support with the biological studies and thank Pamela Winchester for proofreading the manuscript.

Appendix A. Supplementary data

Supplementary data to this article can be found online at https://doi.org/10.1016/j.jconrel.2019.01.035.

References

[1] A. Wicki, D. Witzigmann, V. Balasubramanian, J. Huwyler, Nanomedicine in cancer therapy: challenges, opportunities, and clinical applications, J. Control. Release 200 (2015) 138–157, https://doi.org/10.1016/j.jconrel.2014.12.030.
[2] J. Shi, P.W. Kantoff, R. Wooster, O.C. Farokhzad, Cancer nanomedicine: progress, challenges and opportunities, Nat. Rev. Cancer 17 (2017) 20–37, https://doi.org/10.1038/nrc.2016.108.
[3] R. Esfand, D.A. Tomalia, Poly(amidoamine) (PAMAM) dendrimers: from biomimicry to drug delivery and biomedical applications, Drug Discov. Today 6 (2001) 427–436, https://doi.org/10.1016/S1359-6446(01)01757-3.
[4] J. Li, H. Liang, J. Liu, Z. Wang, Poly (amidoamine) (PAMAM) dendrimer mediated delivery of drug and pDNA/siRNA for cancer therapy, Int. J. Pharm. 546 (2018) 215–225, https://doi.org/10.1016/j.ijpharm.2018.05.045.
[5] V. Paola, G. Antonella, O. Giancarlo, M. Andrea, Polyethylenimine in medicinal chemistry, Curr. Med. Chem. 15 (2008) 2826–2839, https://doi.org/10.2174/092986708786242778.
[6] A.P. Pandey, K.K. Sawant, Polyethylenimine: a versatile, multifunctional non-viral vector for nucleic acid delivery, Mater. Sci. Eng. C 68 (2016) 904–918, https://doi.org/10.1016/j.msec.2016.07.066.
[7] M. Calderón, M.A. Quadir, S.K. Sharma, R. Haag, Dendritic Polyglycerols for biomedical applications, Adv. Mater. 22 (2010) 190–218, https://doi.org/10.1002/adma.200902144.
[8] S. Abbina, S. Vappala, P. Kumar, E.M.J. Siren, C.C. La, U. Abbasi, D.E. Brooks, J.N. Kizhakkedathu, Hyperbranched polyglycerols: recent advances in synthesis, biocompatibility and biomedical applications, J. Mater. Chem. B 5 (2017) 9249–9277, https://doi.org/10.1039/C7TB02515G.
[9] A. Sousa-Herves, P. Würfel, N. Wegner, J. Khandare, K. Licha, R. Haag, P. Welker, M. Calderón, Dendritic Polyglycerol Sulfate as a novel platform for paclitaxel delivery: pitfalls of Ester linkage, Nanoscale 7 (2015) 3923–3932, https://doi.org/10.1039/C4NR04428B.
[10] S. Ferber, G. Tiram, A. Sousa-Herves, A. Eldar-Boock, A. Krivitsky, A. Scomparin, E. Yeini, P. Ofek, D. Ben-Shushan, L.I. Vossen, K. Licha, R. Grossman, Z. Ram, J. Henkin, E. Ruppin, N. Auslander, R. Haag, M. Calderón, R. Satchi-Fainaro, Co-targeting the tumor endothelium and P-selectin-expressing glioblastoma cells leads to a remarkable therapeutic outcome, eLife 6 (2017) e25281, , https://doi.org/10.7554/eLife.25281.
[11] Brentuximab Vedotin, Drugs in R&D, vol. 11, (2011), pp. 85–95, https://doi.org/10.2165/11591070-000000000-00000.
[12] S.O. Doronina, B.E. Toki, M.Y. Torgov, B.A. Mendelsohn, C.G. Cerveny, D.F. Chace, R.L. DeBlanc, R.P. Gearing, T.D. Bovee, C.B. Siegall, J.A. Francisco, A.F. Wahl, D.L. Meyer, P.D. Senter, Development of potent monoclonal antibody auristatin conjugates for cancer therapy, Nat. Biotechnol. 21 (2003) 778–784, https://doi.org/10.1038/nbt832.
[13] C. Batisse, E. Dransart, R. Ait Sarkouh, L. Brulle, S.-K. Bai, S. Godefroy, L. Johannes, F. Schmidt, A new delivery system for auristatin in STxB-drug conjugate therapy, Eur. J. Med. Chem. 95 (2015) 483–491, https://doi.org/10.1016/j.ejmech.2015.03.047.
[14] M. Gund, A. Khanna, N. Dubash, A. Damre, K.S. Singh, A. Satyam, Water-soluble prodrugs of paclitaxel containing self-immolative disulfide linkers, Bioorg. Med. Chem. Lett. 25 (2015) 122–127, https://doi.org/10.1016/j.bmcl.2014.10.088.
[15] C.F. Riber, A.A.A. Smith, A.N. Zelikin, Self-Immolative linkers literally bridge Disulfide chemistry and the realm of Thiol-free drugs, Adv. Healthc. Mater. 4 (2015) 1887–1890, https://doi.org/10.1002/adhm.201500344.
[16] D. Gröger, M. Kerschnitzki, M. Weinhart, S. Reimann, T. Schneider, B. Kohl, W. Wagermaier, G. Schulze-Tanzil, P. Fratzl, R. Haag, Selectivity in bone targeting with multivalent dendritic Polyanion dye conjugates, Adv. Healthc. Mater. 3 (2014) 375–385, https://doi.org/10.1002/adhm.201300205.
[17] K. Licha, P. Welker, M. Weinhart, N. Wegner, S. Kern, S. Reichert, I. Gemeinhardt, C. Weissbach, B. Ebert, R. Haag, M. Schirner, Fluorescence imaging with multifunctional Polyglycerol Sulfates: novel polymeric near-IR probes targeting inflammation, Bioconjug. Chem. 22 (2011) 2453–2460, https://doi.org/10.1021/bc2002727.
[18] S. Biffi, S. Dal Monego, C. Dullin, C. Garrovo, B. Bosnjak, K. Licha, P. Welker, M.M. Epstein, F. Alves, Dendritic Polyglycerolsulfate near infrared fluorescent (NIRF) dye conjugate for non-invasively monitoring of inflammation in an allergic asthma mouse model, PLoS One 8 (2013) 1–9, https://doi.org/10.1371/journal.pone.0057150.
[19] D. Gröger, F. Paulus, K. Licha, P. Welker, M. Weinhart, C. Holzhausen, L. Mundhenk, A.D. Gruber, U. Abram, R. Haag, Synthesis and biological evaluation of radio and dye Labeled amino functionalized dendritic Polyglycerol Sulfates as multivalent anti-inflammatory compounds, Bioconjug. Chem. 24 (2013) 1507–1514, https://doi.org/10.1021/bc400047f.
[20] F. Paulus, R. Schulze, D. Steinhilber, M. Zieringer, I. Steinke, P. Welker, K. Licha, S. Wedepohl, J. Dernedde, R. Haag, The effect of Polyglycerol Sulfate branching on inflammatory processes, Macromol. Biosci. 14 (2014) 643–654, https://doi.org/10.1002/mabi.201300420.
[21] F. Paulus, D. Steinhilber, P. Welker, D. Mangoldt, K. Licha, H. Depner, S. Sigrist, R. Haag, Structure related transport properties and cellular uptake of hyperbranched polyglycerol sulfates with hydrophobic cores, Polym. Chem. 5 (2014) 5020–5028, https://doi.org/10.1039/C4PY00430B.
[22] H.R. Krüger, I. Schütz, A. Justies, K. Licha, P. Welker, V. Haucke, M. Calderón, Imaging of doxorubicin release from theranostic macromolecular prodrugs via fluorescence resonance energy transfer, J. Control. Release 194 (2014) 189–196, https://doi.org/10.1016/j.jconrel.2014.08.018.
[23] K. Kono, C. Kojima, N. Hayashi, E. Nishisaka, K. Kiura, S. Watarai, A. Harada, Preparation and cytotoxic activity of poly(ethylene glycol)-modified poly(amidoamine) dendrimers bearing adriamycin, Biomaterials 29 (2008) 1664–1675, https://doi.org/10.1016/j.biomaterials.2007.12.017.